Methyltrioxorhenium Interactions with Lewis Acid Sites of an Amorphous Silica−Alumina

Anthony W. Moses,[†] Naseem A. Ramsahye,[†] Christina Raab,[†] Heather D. Leifeste,[†] Swarup Chattopadhyay,[†] Bradley F. Chmelka,*[,†] Juergen Eckert,*[,§,⊥] and Susannah L. Scott*[,†,‡]

Departments of Chemical Engineering and Chemistry, University of California, Santa Barbara, California 93106, Materials Research Laboratory, University of California, Santa Barbara, California 93106, and Manual Lujan, Jr., Neutron Scattering Center, Los Alamos National Laboratory, Los Alamos, New Mexico 87545

Received November 9, 2005

Deposition of CH_3ReO_3 onto the dehydrated surface of an amorphous silica−alumina (Si/Al = 4.8) generates a catalyst for olefin metathesis, although CH_3ReO_3 itself is not active. The nature of the interactions between the silica−alumina surface and the grafted organometallic complex was probed by 1D and 2D ^1H, ^{13}C, and ^{27}Al solid-state NMR, IR, EXAFS, and DFT calculations. The methyl ligand remains bound to Re, but grafting alters its symmetry, as well as the shielding of the ^{13}C and ^1H nuclei. Chemisorption of the intact molecular complex occurs via interaction of one oxo ligand with an Al site, resulting in significant elongation of this Re═O bond. Comparison of EXAFS- and DFT-derived bond distances suggests that the participating Lewis acid sites of silica−alumina involve five-coordinate Al. A second surface−organometallic interaction arises by coordination of an adjacent bridging oxygen atom (AlOSi) to the Re center. These insights represent a first step toward understanding the role of solid oxide supports in conferring metathesis activity to CH_3ReO_3 and related heterogeneous catalysts.

Introduction

The mechanisms by which methyltrioxorhenium, CH_3ReO_3, catalyzes the homogeneous epoxidation of olefins and the olefination of aldehydes are now fairly well-understood.[1] In contrast, the origin of its reactivity in olefin metathesis remains unclear, particularly the step in which the initiating carbene is formed. Although tautomerization to $CH_2═ReO_2(OH)$ occurs upon UV irradiation, this carbene is not thermally accessible,[2,3] and CH_3ReO_3 shows no reactivity toward olefins in solution. Metathesis activity is conferred by interaction with a Lewis acid, either soluble (e.g., R_nAlCl_{3-n}, $AlCl_3$, or $AlCl_3/SnMe_4$)[4,5] or solid (e.g., silica−alumina, alumina, niobia, or zeolite Y).[5−8] Interestingly, a methylene tautomer of CH_3ReO_3 was formed in the presence of $SnMe_2Cl_2$ by trapping with pyridine;[9] however, no reactivity for the product was reported.

Early accounts presented conflicting evidence for direct involvement of a carbene tautomer of Lewis-acid-activated CH_3ReO_3 in metathesis. In a study of 1-butene homometathesis catalyzed by CD_3ReO_3 supported on silica−alumina, the deuterium label was incorporated in the olefinic products as both $CD_2═CHCH_2CH_3$ and $CD_2═CH_2$.[5] Reaction of *trans*-2,5-dimethyl-3-hexene with $^{13}CH_3ReO_3$ supported on niobia produced 3-methyl-1-butene, the expected product of a metathesis reaction with a carbene site $Re═CH_2$, but the olefin contained less than 5% of the ^{13}C-label.[10] However, the mechanisms of D and ^{13}C transfer to olefin may differ; furthermore, CH_3ReO_3 may not interact in the same way with the different oxide supports, since niobia, unlike silica−alumina, readily exhibits oxygen nonstoichiometry.[11]

Even the structure of grafted CH_3ReO_3 remains obscure. Metathesis activity was correlated with Lewis acidity for the $^{13}CH_3ReO_3$/niobia catalyst,[6] although no model for the grafted site was proposed. On silica−alumina, grafting of CH_3ReO_3 via condensation with a pair of adjacent surface hydroxyl groups was assumed,[5] by analogy to the homogeneous reactions of CH_3ReO_3 with diols.[12−14] A DFT calculation showed such a condensation reaction with the molecular disilanol $H_2Si(OH)$-

* To whom correspondence should be addressed. E-mail: bradc@engineering.ucsb.edu; juergen@mrl.ucsb.edu; sscott@engineering.ucsb.edu. Fax: 1-805-893-4731.

† Department of Chemical Engineering, University of California.

‡ Department of Chemistry, University of California.

§ Materials Research Laboratory, University of California.

⊥ Los Alamos National Laboratory.

(1) Kühn, F.; Scherbaum, A.; Herrmann, W. A. *J. Organomet. Chem.* **2004**, *689*, 4149−4164.

(2) Morris, L. J.; Downs, A. J.; Greene, T. M.; McGrady, G. S.; Herrmann, W. A.; Sirsch, P.; Gropen, O.; Scherer, W. *Chem. Commun.* **2000**, 67−68.

(3) Morris, L. J.; Downs, A. J.; Greene, T. M.; McGrady, G. S.; Herrmann, W. A.; Srisch, P.; Scherer, W.; Gropen, O. *Organometallics* **2001**, *20*, 2344−2352.

(4) Herrmann, W. A.; Kuchler, J. G.; Wagner, W.; Felixberger, J. K.; Herdtweck, E. *Angew. Chem., Int. Ed. Engl.* **1988**, *27*, 394−396.

(5) Herrmann, W. A.; Wagner, W.; Flessner, U. N.; Volkhardt, U.; Komber, H. *Angew. Chem., Int. Ed. Engl.* **1991**, *30*, 1636−1638.

(6) Buffon, R.; Auroux, A.; Lefebvre, F.; Leconte, M.; Choplin, A.; Basset, J. M.; Herrmann, W. A. *J. Mol. Catal.* **1992**, *76*, 287−295.

(7) Rost, A. M. J.; Schneider, H.; Zoller, J. P.; Herrmann, W. A.; Kühn, F. E. *J. Organomet. Chem.* **2005**, *690*, 4712−4718.

(8) Bein, T.; Huber, C.; Moller, K.; Wu, C.-G.; Xu, L. *Chem. Mater.* **1997**, *9*, 2252−2254.

(9) Zhang, C.; Guzei, I. A.; Espenson, J. A. *Organometallics* **2000**, *19*, 5257−5259.

(10) Basset, J. M.; Buffon, R.; Choplin, A.; Leconte, M.; Tourode, R.; Herrmann, W. A. *J. Mol. Catal.* **1992**, *72*, L7−L10.

(11) Nowak, I.; Ziolek, M. *Chem. Rev.* **1999**, *99*, 3603−3624.

(12) Takacs, J.; Cook, M. R.; Kiprof, P.; Kuchler, J. G.; Herrmann, W. A. *Organometallics* **1991**, *10*, 316−320.

(13) Takacs, J.; Kiprof, P.; Riede, J.; Herrmann, W. A. *Organometallics* **1990**, *9*, 782−787.

(14) Herrmann, W. A.; Watzlowik, P.; Kiprof, P. *Chem. Ber.* **1991**, *124*, 1101−1106.

10.1021/om050962k CCC: $33.50
Publication on Web 03/30/2006

$OSi(OH)H_2$ to be endothermic.[3] Nevertheless, subsequent tautomerization of the silanolate complex was proposed, aided by relaxation of the silica surface via protolytic opening of a strained siloxane ring.

Understanding the CH_3ReO_3−support interaction is the first step toward explaining how heterogeneous rhenium-based catalysts acquire their unique metathesis activity: both CH_3ReO_3 on silica−alumina[5,7,15] and alumina-supported perrhenates promoted by SnR_4[16] are capable of transforming even functionalized olefins at room temperature. In this report, we combine spectroscopic and computational analysis to establish the nature of the energetically favored grafted CH_3ReO_3 sites on silica−alumina.

Experimental Section

Materials. The silica−alumina used in this work, Davicat 3113 (7.6 wt % Al (dry basis), BET surface area 573 m^2/g, pore volume 0.76 cm^3/g), was provided by Grace-Davison (Columbia, MD). In each experiment, the appropriate amount of silica−alumina was first outgassed in a Pyrex reactor for 4 h at 450 °C under dynamic vacuum ($\leq 10^{-4}$ Torr), then calcined for 12 h under 350 Torr static O_2 at the same temperature, and allowed to cool to room temperature under dynamic vacuum. The choice of 450 °C was dictated by the minimum temperature required to remove adsorbed water, hydrocarbon impurities, and surface carbonates during the calcination step. The resulting material will be referred to as "dehydrated silica−alumina", since spectroscopic signals characteristic of adsorbed water (IR: 1640 cm^{-1}; ^1H MAS NMR: 6.4 ppm)[17] disappear when silica−alumina is treated under vacuum at temperatures above 340 °C.[18]

Volatile CH_3ReO_3 (Aldrich) was sublimed at 10^{-4} Torr and room temperature into a reactor containing dehydrated silica−alumina powder, while the solid was shaken vigorously to promote its uniform exposure to the volatile organometallic complex and thus macroscopic sample homogeneity. In addition, the targeted loading of CH_3ReO_3 was kept well below its maximum chemisorption uptake on this silica−alumina, ca. 10 wt % Re, to enhance the local uniformity of the grafted sites. No physisorbed material was recovered from CH_3ReO_3/silica−alumina samples prepared with <10 wt % Re loading upon subjecting them to prolonged desorption to a liquid N_2 trap at room temperature under vacuum. Consequently, the desorption step was omitted in many experiments, with no discernible effect on the spectra or the catalytic activity (to be reported separately). To minimize materials transfers and ensure sample integrity, a new batch of the highly air-sensitive grafted CH_3ReO_3 was made for each measurement (with the exception of sequential NMR experiments); therefore, the weight loading varied from sample to sample (typically 1−2 wt %). To enhance sensitivity in ^{13}C CPMAS NMR experiments, labeled $^{13}CH_3ReO_3$ (>99% ^{13}C) was prepared from $^{13}CH_3SnBu_3$, according to a literature procedure.[3,19]

Rhenium Analysis. Re loadings were determined by quantitative extraction, followed by UV spectrophotometric analysis. Samples containing ca. 30 mg of silica−alumina and <3 wt % Re were first weighed in an inert atmosphere. (The mass of dehydrated silica−alumina increases up to 15% upon exposure to air, due to adsorption of atmospheric moisture.) Re was extracted as perrhenate by stirring overnight in air with 5 mL of 3 M NaOH. Samples were diluted to 25 mL with 3 M H_2SO_4 and filtered, and their UV spectra were recorded on a Shimadzu UV2401PC spectrophotometer. Re concentration was determined at 224 nm, using a calibration curve prepared with NH_4ReO_4 (Aldrich).

Solid-State NMR. All experiments were performed at room temperature on a Bruker AVANCE 300 NMR spectrometer operating at 300.1010 MHz for ^1H, 75.4577 MHz for ^{13}C, and 78.2067 MHz for ^{27}Al. The highly air-sensitive samples were packed under an argon atmosphere, in a glovebox equipped with O_2- and moisture-sensors, into zirconia MAS rotors with tightly fitting caps sealed with Viton R O-rings (Wilmad). Spectra were acquired with a 4 mm broadband MAS probehead in rotors spinning at 12 kHz. The absence of adventitious moisture was confirmed regularly by the lack of a discernible peak at 6.4 ppm in ^1H MAS NMR spectra.[17]

Single-pulse ^1H MAS experiments were performed with a 90° pulse length of 3.7 μs, an acquisition time of 25 ms, and a recycle delay of 3 s. For quantitative ^1H MAS NMR, 60 mg of dehydrated silica−alumina was weighed in an atmosphere of dry N_2. A small piece of poly(dimethylsiloxane) (PDMS, ca. 1 mg, weighed to within ±0.05 mg) was used as an internal standard for quantifying ^1H NMR signal intensities. PDMS was chosen because it exhibits a single signal with an isotropic ^1H chemical shift of −0.1 ppm (relative to TMS) that does not overlap with the signals of interest.[20] Spectra were deconvoluted using the program DMFIT, to obtain Gaussian fits to spectral line shapes.[21]

^{13}C CPMAS spectra were recorded using a 90° pulse length of 3.5 μs, a contact time of 3 ms, an acquisition time of 21 ms, and a recycle delay of 2 s. Because of the low carbon content of the samples, signal intensity was enhanced by use of ^{13}C-labeled CH_3ReO_3. Both ^1H and ^{13}C chemical shifts were referenced to tetramethylsilane (TMS). The same experimental conditions were used in the two-dimensional (2D) $^{13}C\{^1H\}$ heteronuclear chemical shift correlation (HETCOR) experiment. For each of the 256 t_1 increments, 128 acquisitions were collected with a 2 s recycle delay. During the detection period t_2, 1024 points were collected with a dwell time of 20 μs. The outer contour level is drawn at 45% of the maximum intensity. Lower 2D intensity thresholds down to 2% revealed no additional correlations beyond those shown in Figure 3.

Single-pulse ^{27}Al MAS experiments were performed with a 90° pulse length of 3.8 μs, an acquisition time of 4.1 ms, and a recycle delay of 15 s. Chemical shifts were referenced to an aqueous solution of $Al(NO_3)_3$ as an external standard. A small piece of dense AlN (2.3 mg, containing 0.057 mmol of Al) was used as an internal "spin-counting" standard to quantify ^{27}Al MAS signal intensities. AlN was chosen because its isotropic signal at 113 ppm does not overlap with the ^{27}Al signals of interest, and a spinning speed of 14 kHz was used to avoid overlap with the ^{27}AlN spinning sidebands. A recycle delay of 15 s was used to allow for the long spin−lattice relaxation time of polycrystalline AlN.[22] A total of 16 000 scans were acquired for each ^{27}Al spectrum. Spectra were subsequently deconvoluted with DMFIT, using Gaussian fits and including spinning sidebands for comparison of integrated ^{27}Al peak areas.[21]

Infrared Spectroscopy. The IR spectrum of polycrystalline CH_3ReO_3 was obtained by pressing with KBr into a self-supporting pellet. The IR grafting experiment was performed in vacuo in a Pyrex cell equipped with KCl windows affixed with TorrSeal (Varian). Its high-vacuum ground-glass stopcock and joints were lubricated with Apiezon H grease (Varian). A self-supporting pellet

(15) Mathew, T. M.; du Plessis, J. A. K.; Prinsloo, J. J. *J. Mol. Catal. A: Chem.* **1999**, *148*, 157−164.
(16) Mol, J. C. *Catal. Today* **1999**, *51*, 289−299.
(17) Hunger, M.; Freude, D.; Pfeifer, H. *J. Chem. Soc., Faraday Trans.* **1991**, *87*, 657−662.
(18) Bronnimann, C. E.; Chuang, I. S.; Hawkins, B. L.; Maciel, G. E. *J. Am. Chem. Soc.* **1987**, *109*, 1562−1564.
(19) Herrmann, W. A.; Kuehn, F. E.; Fischer, R. W.; Thiel, W. R.; Romao, C. C. *Inorg. Chem.* **1992**, *31*, 4431−4432.
(20) Liu, C. C.; Maciel, G. E. *Anal. Chem.* **1996**, *68*, 1401−1407.
(21) Massiot, D.; Fayon, F.; Capron, M.; King, I.; Calvé, S. L.; Alonso, B.; Durand, J.-O.; Bujoli, B.; Gan, Z.; Hoatson, G. *Magn. Reson. Chem.* **2002**, *40*, 70−76.
(22) Haase, J.; Freude, D.; Frölich, T.; Himpel, G.; Kerbe, F.; Lippmaa, E.; Pfeifer, H.; Sarv, P.; Schäfer, H.; Seiffert, B. *Chem. Phys. Lett.* **1989**, *156*, 328−332.

of silica−alumina was prepared in air by pressing ca. 25 mg of material at 40 kg/cm^2 in a 16 mm stainless steel die and was transferred to a Pyrex pellet holder. Sublimation of CH_3ReO_3 via a vacuum manifold directly onto a silica−alumina pellet in the presence of TorrSeal led to unwanted side-reactions of the latter with the organometallic complex. Instead, the pellet was calcined and dehydrated in an all-glass Schlenk tube, exposed to CH_3ReO_3 by sublimation, then transferred to the IR cell under argon in a glovebox. The IR spectrum of the self-supporting pellet was recorded in vacuo in transmission mode. IR spectra were recorded on a Shimadzu PrestigeIR spectrophotometer equipped with a DTGS detector and purged with CO_2-free dry air from a Balston 75-52 purge gas generator. Background and sample spectra were recorded by co-adding 64 scans at a resolution of 4 cm^{-1}.

Density Functional Theory Calculations. Computations were performed on an Intel Xeon computer running Linux, as well as the VRANA-5 and VRANA-8 clusters at the Center for Molecular Modeling of the National Institute of Chemistry (Ljubljana, Slovenia), using the DFT implementation in the Gaussian03 code, Revision C.02.[23] The orbitals were described by a mixed basis set. A fully uncontracted basis set from LANL2DZ was used for the valence electrons of Re,[24] augmented by two f functions ($\zeta = 1.14$ and 0.4) in the full optimization. Re core electrons were treated by the Hay−Wadt relativistic effective core potential (ECP) given by the standard LANL2 parameter set (electron−electron and nucleus−electron). The 6-31G** basis set was used to describe the rest of the system. It is well-established for use with organic molecules and has also been shown to reproduce experimentally determined aluminosilicate structures.[25] The B3PW91 density functional was used in all calculations.

X-ray Absorption Spectroscopy. Spectra were recorded at the Re L_{III} edge (10 535 eV) at the Stanford Synchrotron Radiation Laboratory on beamline 2-3 (bend), operating at 3.0 GeV with a current of 75−100 mA. X-rays were monochromatized via reflection from a pair of Si(111) crystals through a 1 mm entrance slit. The incident beam was detuned 30% to suppress harmonics. Samples were mounted at a 45° angle to the beam in order to collect transmission and fluorescence spectra simultaneously. The intensity of the incident beam was measured with a N_2-filled ion chamber detector installed in front of the sample. Transmitted X-rays were detected in a second, N_2-filled ion chamber. Fluorescence from the sample was recorded at right angles to the beam, by an Ar-filled Lytle detector installed without Soller slits.

Powder samples were packed in 35 × 5 × 2 mm slots in aluminum sample plates with windows of 12.0 μm polypropylene film (Chemplex #475) affixed with double-sided tape to each side of the plate. This sample preparation technique has been shown to prevent even highly air-sensitive samples from decomposing.[26] To avoid spectral artifacts due to sample thickness,[27] the sample of polycrystalline CH_3ReO_3 was diluted to ca. 3 wt % Re by mixing the solid with powdered boron nitride (Strem) in air. Highly air-sensitive CH_3ReO_3/silica−alumina was packed, without dilution, into the sample plate under N_2. A single data sweep (collection time ∼20 min) was sufficient to obtain a good signal-to-noise ratio in the fluorescence channel. Subsequent data sweeps showed no change due to sample decomposition. Fluorescence data generally showed better signal-to-noise ratios and were used in subsequent data analyses instead of transmission data.

EXAFS spectra were analyzed in *k*-space using WinXAS v.3.1.[28] The data were first background-corrected by subtracting a linear fit to the pre-edge region extrapolated the entire length of the spectrum, then normalized by a third-degree polynomial fitted to the post-edge region. EXAFS spectra were *k*-weighted and fitted with a polynomial spline with 4 knots between 2 and 14 Å^{-1}. Subtraction of this spline minimizes contributions from low-frequency atomic X-ray absorption fine structure (AXAFS).[29] A Kaiser-Bessel window function ($\alpha = 4$) was applied to the data range prior to Fourier transformation, to minimize spectral ringing. Only single-scattering paths in the EXAFS equation, eq 1, were fitted to the *k*-space spectra with least-squares refinement:[30]

$$\chi(k) = S_0^2 \sum_i \frac{N_i F_i(k)}{kR_i^2} \exp(-2k^2\sigma_i^2) \exp\left(\frac{-2R_i}{\lambda(k)}\right) \sin(2kR_i + \phi_i(k)) \quad (1)$$

where N_i is the number of scatterers in the *i*th shell at a distance *R* from the absorber. The Debye−Waller factor, σ_i^2, is the root-mean-squared relative displacement of the scatterer, $\lambda(k)$ is the mean-free path of the photoelectron, and $\phi(k)_i$ and $F(k)_i$ are the phase shift and backscattering amplitude, respectively. The phase shift and backscattering amplitude functions were calculated using FEFF 8.20.[31] Since curve-fitting was performed using a priori electronic calculations, no reference spectra were needed or used in the EXAFS analysis.

The EXAFS equation has a large number of degrees of freedom, and some of its parameters are strongly correlated. During curve-fitting, all parameters were not permitted to vary simultaneously. Since each model involves a well-defined organometallic complex as its starting point, coordination numbers were initially fixed at their corresponding integer values. Path lengths and Debye−Waller factors were then allowed to vary sequentially, while S_0^2 and ΔE_0 were held fixed, until the residual changed by <1%. The fitted values were then fixed, while S_0^2 and ΔE_0 were sequentially refined. Goodness-of-fit was evaluated via the magnitude of the residual, defined as $\sum(y_{obs}(i) - y_{fit}(i))/\sum y_{obs}(i)$, where $y_{obs}(i)$ and $y_{fit}(i)$ are the observed and calculated values of each (unweighted) data point in *k*-space, as well as the appropriateness of the fit parameters (path lengths, Debye−Waller factors). The total number of independent fitted parameters may not exceed N_{idp}, given by eq 2:[32]

$$N_{idp} = \frac{2\Delta k \Delta R}{\pi} \quad (2)$$

where Δk and ΔR are the ranges over which the data are substantial (i.e., containing features distinguishable from the noise) in *k*-space and *R*-space, respectively.

(23) Frisch, M. J.; Trucks, G. W.; Schlegel, H. B.; Scuseria, G. E.; Robb, M. A.; Cheeseman, J. R.; Montgomery, J. A., Jr.; Vreven, T.; Kudin, K. N.; Burant, J. C.; Millam, J. M.; Iyengar, S. S.; Tomasi, J.; Barone, V.; Mennucci, B.; Cossi, M.; Scalmani, G.; Rega, N.; Petersson, G. A.; Nakatsuji, H.; Hada, M.; Ehara, M.; Toyota, K.; Fukuda, R.; Hasegawa, J.; Ishida, M.; Nakajima, T.; Honda, Y.; Kitao, O.; Nakai, H.; Klene, M.; Li, X.; Knox, J. E.; Hratchian, H. P.; Cross, J. B.; Bakken, V.; Adamo, C.; Jaramillo, J.; Gomperts, R.; Stratmann, R. E.; Yazyev, O.; Austin, A. J.; Cammi, R.; Pomelli, C.; Ochterski, J. W.; Ayala, P. Y.; Morokuma, K.; Voth, G. A.; Salvador, P.; Dannenberg, J. J.; Zakrzewski, V. G.; Dapprich, S.; Daniels, A. D.; Strain, M. C.; Farkas, O.; Malick, D. K.; Rabuck, A. D.; Raghavachari, K.; Foresman, J. B.; Ortiz, J. V.; Cui, Q.; Baboul, A. G.; Clifford, S.; Cioslowski, J.; Stefanov, B. B.; Liu, G.; Liashenko, A.; Piskorz, P.; Komaromi, I.; Martin, R. L.; Fox, D. J.; Keith, T.; Al-Laham, M. A.; Peng, C. Y.; Nanayakkara, A.; Challacombe, M.; Gill, P. M. W.; Johnson, B.; Chen, W.; Wong, M. W.; Gonzalez, C.; Pople, J. A. *Gaussian 03*, revision C.02; Gaussian, Inc.: Wallingford, CT, 2004.

(24) Pietsch, M. A.; Russo, T. V.; Murphy, R. B.; Martin, R. L.; Rappe, A. K. *Organometallics* **1998**, *17*, 2716−2719.

(25) Nedelec, J. M.; Hench, L. L. *J. Non-Cryst. Solids* **2000**, *277*, 106−113.

(26) Deguns, E. W.; Taha, Z.; Meitzner, G.; Scott, S. L. *J. Phys. Chem. B* **2005**, *109*, 5005−5011.

(27) Meitzner, G. *Catal. Today* **1998**, *39*, 281−291.

(28) Ressler, T. *J. Synchrotron Rad.* **1998**, *5*, 118−122.

(29) Wang, W. C.; Chen, Y. *Phys. Status Solidi A* **1998**, *168*, 351−357.

(30) Sayers, D. E.; Stern, E. A.; Lytle, F. W. *Phys. Rev. Lett.* **1971**, *27*, 1204−1207.

(31) Ankudinov, A. L.; Bouldin, C.; Rehr, J. J.; Sims, J.; Hung, H. *Phys. Rev. B* **2002**, *65*, 104107.

(32) In *X-Ray Absorption Fine Structure*; Hashain, S. S., Ed.; Ellis Horwood: New York, 1991; pp 751−770.

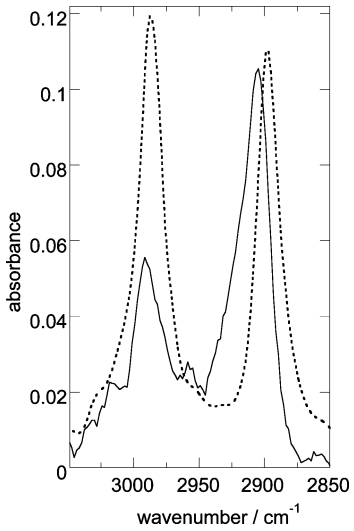

Figure 1. Comparison of FTIR spectra for polycrystalline CH_3ReO_3 (as KBr pellet, dashed line) and CH_3ReO_3 grafted on silica−alumina (2.3 wt % Re, solid line), in the $\nu(CH_3)$ region.

Results and Discussion

Adsorption of CH_3ReO_3 onto amorphous, dehydrated, and partially dehydroxylated silica−alumina (7.6 wt % Al) was achieved at room temperature from the vapor phase. Chemisorption is rapid and irreversible: up to 10 wt % Re can be deposited without subsequent loss of CH_3ReO_3 during prolonged evacuation at room temperature ($\leq 10^{-4}$ Torr). In the experiments described below, the loading of CH_3ReO_3 was kept much lower ($\leq$2.3 wt % Re), to promote the structural uniformity of the grafted sites on the amorphous silica−alumina support.[33]

No volatiles (e.g., CH_4) were detected by either GC or FTIR during grafting, for any Re loading. At loadings higher than 1 wt % Re, the white silica−alumina acquired a distinctly yellow-brown color that was stable under room light, but bleached rapidly upon exposure to air. The IR spectrum confirms that the methyl group remained intact upon grafting. The $\nu_{as}(CH_3)$ and $\nu_s(CH_3)$ modes shift slightly, from 2989 and 2900 cm^{-1} to 2993 and 2907 cm^{-1}, respectively, Figure 1, and their relative intensities change, compared to the IR spectrum of polycrystalline CH_3ReO_3.[34] The $\delta_{as}(CH_3)$ mode also shifts from 1374 to 1370 cm^{-1}. These results suggest that the symmetry at Re (and, consequently, of the methyl group) changes as a consequence of its adsorption.

Solid-State NMR Analyses. Since NMR chemical shifts are sensitive to local structure(s) in grafted metal complexes, they can be used to assess the environment of the methyl group in the adsorbed organorhenium complex. The ^{13}C CPMAS spectrum of $^{13}CH_3ReO_3$ grafted onto dehydrated silica−alumina (0.4 wt % Re) consists of a single isotropic signal at 29 ppm, Figure 2a. This chemical shift is consistent with retention of the methyl group at Re in the grafted complex; however, the electronic structure of the grafted site is clearly different from the isolated molecule, since the ^{13}C spectrum of CH_3ReO_3 in $CDCl_3$ contains a single peak at 19 ppm.[35]

The single-pulse ^1H MAS NMR spectrum of the unmodified, dehydrated silica−alumina is shown in Figure 2b. The peak at

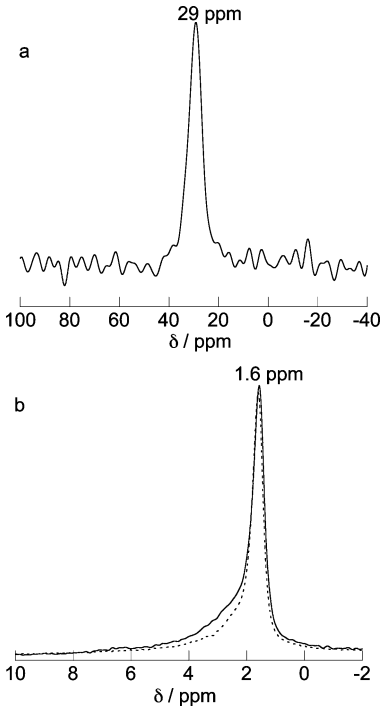

Figure 2. (a) ^{13}C CPMAS spectrum for silica−alumina modified with $^{13}CH_3ReO_3$ (0.4 wt % Re) and (b) single-pulse ^1H MAS NMR spectra of dehydrated silica−alumina before (dashed line) and after (solid line) modification with $^{13}CH_3ReO_3$ (0.4 wt % Re). Spinning rate 12 kHz.

1.6 ppm and its downfield shoulder at 2.3 ppm are attributed to isolated (noninteracting), terminal silanol groups,[18,36] with a distribution of acidities and hence chemical shifts.[17] No signals for terminal AlOH groups (ca. 1 ppm), bridging AlO(H)Al groups (2.5−3.6 ppm), or zeolite-like bridging hydroxyls AlO(H)Si were observed (3.8−4.4 ppm),[17,37,38] in agreement with literature reports that all protons in silica-rich amorphous silica−aluminas are associated with silanol sites.[36,39] After grafting $^{13}CH_3ReO_3$ onto the dehydrated silica−alumina support (0.4 wt % Re), the ^1H MAS spectrum retained the strong signals of the silanol protons, whose chemical shifts are virtually unchanged relative to the unmodified support, Figure 2b. The downfield shoulder is slightly broader and more intense, consistent with the presence of an additional signal at ca. 3 ppm from the methyl protons of the grafted complex (see below). For comparison, the ^1H spectrum of CH_3ReO_3 in $CDCl_3$ consists of a single peak at 2.64 ppm.

A two-dimensional (2D) $^{13}C\{^1H\}$ HETCOR MAS NMR experiment was used to locate the ^1H signal due to adsorbed CH_3ReO_3. The HETCOR contour plot, Figure 3, shows a strong intensity correlation between the ^{13}C and ^1H signals at 29 and 2.8 ppm, respectively, establishing that a weak ^1H signal at this position corresponds to the methyl protons of grafted CH_3ReO_3. Furthermore, the absence of intensity correlation between the ^{13}C methyl signal and the signal at 1.6 ppm demonstrates that dipole−dipole couplings between the methyl and hydroxyl protons were weak during the 3 ms contact time and suggests that most grafted CH_3ReO_3 sites are not within molecular proximity of these silanol sites at this low Re loading. In contrast, studies of the adsorption of CH_3ReO_3 in zeolite HY

(33) At higher loadings, the grafting sites are less uniform. The origin of this complexity will be described separately.

(34) Mink, J.; Keresztury, G.; Stirling, A.; Herrmann, W. A. *Spectrochim. Acta, Part A* **1994**, *50*, 2039−2057.

(35) Herrmann, W. A.; Kiprof, P.; Rypdal, K.; Tremmel, J.; Blom, R.; Alberto, R.; Behm, J.; Albach, R. W.; Bock, H.; Solouki; Mink, J.; Lichtenberger, D.; Gruhn, N. E. *J. Am. Chem. Soc.* **1991**, *113*, 6527−6537.

(36) Gun'ko, V. M.; Turov, V. V. *Langmuir* **1999**, *15*, 6405−6415.

(37) Fleischer, U.; Kutzelnigg, W.; Bleiber, A.; Sauer, J. *J. Am. Chem. Soc.* **1993**, *115*, 7833−7838.

(38) Hunger, M. *Solid State Nucl. Magn. Reson.* **1996**, *6*, 1−29.

(39) Schreiber, L. B.; Vaughan, R. W. *J. Catal.* **1975**, *40*, 226−235.

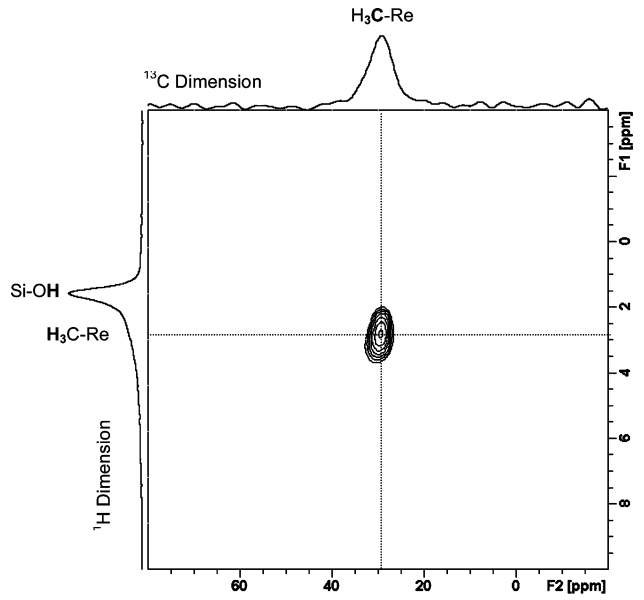

Figure 3. Two-dimensional $^{13}C\{^1H\}$ HETCOR MAS NMR spectrum for silica−alumina modified with $^{13}CH_3ReO_3$ (0.4 wt % Re). The corresponding 1D ^{13}C CPMAS and single-pulse ^1H MAS NMR spectra are plotted along their respective axes.

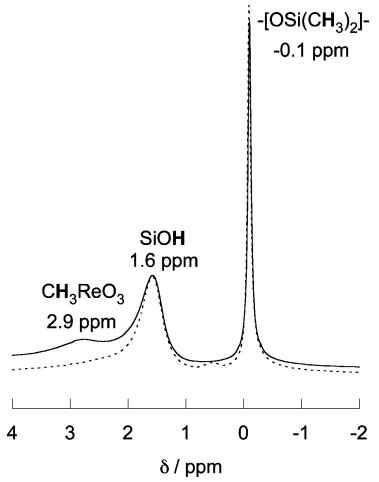

Figure 4. Single-pulse ^1H MAS spectra for the same quantity (60 mg) of the dehydrated silica−alumina support before (dashed line) and after (solid line) grafting CH_3ReO_3 (2.3 wt % Re). A small piece of PDMS (0.1 mg, −0.1 ppm) was included as an internal intensity standard.

concluded that H-bonding between an oxo ligand and an internal hydroxyl group was the main grafting mechanism.[8,40]

Quantitative analyses of the single-pulse ^1H MAS NMR spectra of silica−alumina before and after deposition of CH_3ReO_3 were also performed, to investigate further whether the surface hydroxyl groups are involved in the grafting process. Integrated ^1H peak areas were compared to that of the well-resolved ^1H signal at −0.1 ppm of PDMS, a small (ca. 1 mg) piece of which was added as an internal intensity standard. Within the uncertainty of the NMR measurements (±5%), the intensity of the hydroxyl ^1H peak remains unchanged in the presence of 2.3 wt % Re, Figure 4, indicating that surface hydroxyls are not consumed during grafting. On the basis of the quantitative ^1H MAS spectrum, the hydroxyl content of the dehydrated silica−alumina is estimated to be 2.0 ± 0.2 OH/nm^2, consistent with a previously reported literature value.[20]

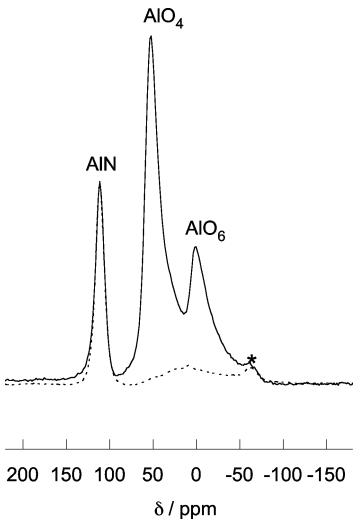

Figure 5. ^{27}Al MAS NMR spectra for hydrated silica−alumina (solid line) and dehydrated silica−alumina (dashed line), recorded in the presence of bulk aluminum nitride (2.3 mg, 113 ppm) as an internal standard. The superimposed spectra were acquired with the same amount of sample (dry basis) and identical experimental parameters and conditions (spinning speed, 14 kHz). * denotes a spinning sideband of AlN.

Also, the ^1H signal of grafted CH_3ReO_3 is clearly seen at 2.9 ppm in Figure 4, due to the higher Re loading.

These experiments indicate that grafting of CH_3ReO_3 does not involve the surface silanols of silica−alumina, at least at low Re loadings. We propose instead that CH_3ReO_3 adsorbs selectively on Lewis acidic Al sites. Quantitative ^{27}Al MAS NMR measurements were performed using the signal at 113 ppm from a small (2.3 mg) piece of ^{27}AlN as an internal intensity standard. Figure 5 shows the spectrum of hydrated silica−alumina (5.7 wt % Al). In addition to the AlN signal at 113 ppm, there are two ^{27}Al peaks at 55 and 2 ppm, with relative intensities of 1.5:1. They are assigned to four- and six-coordinate AlO_x sites, respectively.[41] After dehydration at 450 °C for 12 h, a dramatic reduction (ca. 90%) in ^{27}Al signal intensity occurred under otherwise identical measurement conditions (same quantity of sample on a water-free basis, same NMR acquisition parameters, etc.), Figure 5. This loss of ^{27}Al signal intensity is attributed to the presence of locally distorted Al environments that have large quadrupolar coupling interactions and give rise to very broad signals, as has been reported for dehydrated zeolite[42] and MCM-41-type[43] materials.

Grafting CH_3ReO_3 onto dehydrated silica−alumina resulted in no detectable change in the ^{27}Al MAS spectrum, relative to the spectrum of the dehydrated support before grafting. This result is consistent with association of CH_3ReO_3 with the distorted, low-symmetry ^{27}Al sites, whose resulting coordination number is therefore not directly revealed and remains a challenging characterization objective.

X-ray Absorption Spectroscopy (XAS). The nature of CH_3ReO_3 binding to silica−alumina was investigated by analysis of the Re L_{III}-edge EXAFS. The EXAFS spectrum of polycrystalline CH_3ReO_3 is shown in Figure 6. An EXAFS fit was performed for the first scattering shell (only) of polycrystalline CH_3ReO_3, using literature values for its bond distances[35]

(40) Malek, A.; Ozin, G. A. *Adv. Mater.* **1995**, *7*, 160−163.

(41) McManus, J.; Ashbrook, S. E.; MacKenzie, K. J. D.; Wimperis, S. *J. Non-Cryst. Solids* **2001**, *282*, 278−290.

(42) Fyfe, C. A.; Bretherton, J. L.; Lam, L. Y. *J. Am. Chem. Soc.* **2001**, *123*, 5285−5291.

(43) Janicke, M. T.; Landry, C. C.; Christiansen, S. C.; Birtalan, S.; Stucky, G. D.; Chmelka, B. F. *Chem. Mater.* **1999**, *11*, 1342−1351.

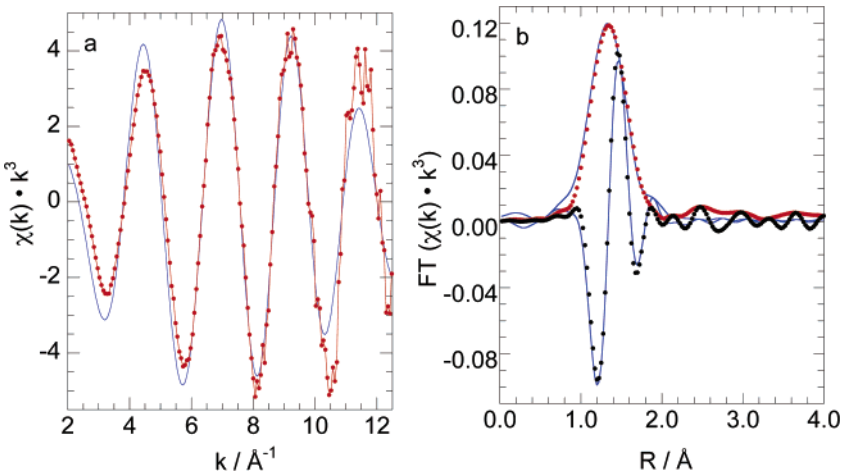

Figure 6. EXAFS data in (a) k^3-weighted k-space (red points and line) and (b) non-phase-corrected R-space (imaginary, black points; FT magnitude, red points) for polycrystalline CH_3ReO_3 diluted in BN (3 wt % Re). Parameters for the curve-fit (blue lines) are given in Table 1.

Table 1. Comparison of Bond Distances (Å) Reported for CH_3ReO_3

path	N	EXAFS curve-fit[a]	DFT calculation[b]	gas-phase electron diffraction[35]	neutron powder diffraction[44]
Re═O	3	1.71 (0.0032)	1.690	1.709	1.702, 1.702, 1.709
Re−C	1	2.11 (0.0028)	2.068	2.060	2.063

[a] This work, for polycrystalline CH_3ReO_3 diluted to 3 wt % Re in BN. Coordination numbers were held fixed at integer values; Debye−Waller factors σ^2 (Å^2) are shown in parentheses. $S_0^2 = 0.98$; $\Delta E_0 = 0.8$ eV; residual = 13.6. [b] This work, for the isolated molecule.

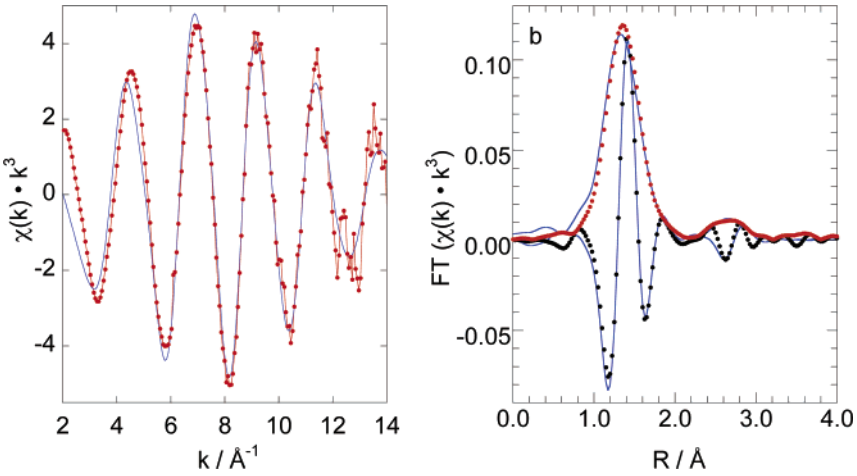

Figure 7. EXAFS data in (a) k^3-weighted k-space (red points and line) and (b) non-phase-corrected R-space (imaginary, black points; FT magnitude, red points) for CH_3ReO_3 adsorbed on dehydrated silica−alumina (1.3 wt % Re). Parameters for the curve-fit (blue lines) with integer coordination numbers are given in Table 2.

as the model starting point. EXAFS fit parameters for polycrystalline CH_3ReO_3 are compared in Table 1 to experimentally determined distances obtained by gas-phase electron diffraction[35] and neutron powder diffraction.[44] The close agreement lends confidence in our method of EXAFS data analysis. The magnitudes of the fitted Debye−Waller factors confirm that polycrystalline CH_3ReO_3 contains a single site with respect to the Re coordination environment. The fitted values are of the same order of magnitude as those reported for other well-defined, single-site materials, as well as those calculated using the vibrational force constants for each single-scattering path, $(1-3) \times 10^{-3}$ Å^2.

After optimization of path lengths and Debye−Waller factors, the global amplitude reduction factor S_0^2 and the inner potential energy ΔE_0 were allowed to vary from their initial values of 1.0 and 0.0, respectively. The fit returned values of 0.98 and 0.80 eV, respectively, and improved the goodness-of-fit only slightly. Path lengths and corresponding Debye−Waller factors were unchanged.

When CH_3ReO_3 is grafted onto silica−alumina, the Re EXAFS changes, Figure 7. Notably, a reproducible feature is visible in non-phase-corrected R-space at ca. 2.7 Å. The appearance of this peak implies a high degree of uniformity in the grafted CH_3ReO_3 sites, i.e., the presence of a well-ordered shell in the second coordination sphere of Re. Such a shell suggests either a highly specific interaction between CH_3ReO_3 and the silica−alumina surface or aggregation of CH_3ReO_3 (although no such feature was observed in the EXAFS of polycrystalline CH_3ReO_3).

Our starting point for curve-fitting the EXAFS spectrum of grafted CH_3ReO_3 used isolated CH_3ReO_3 as the model, with

(44) Herrmann, W. A.; Scherer, W.; Fischer, R. W.; Blümel, J.; Kleine, M.; Mertin, W.; Gruehn, R.; Mink, J.; Boysen, H.; Wilson, C. C.; Ibberson, R. M.; Bachmann, L.; Mattner, M. *J. Am. Chem. Soc.* **1995**, *117*, 3231−3243.

Table 2. Comparison of EXAFS Path Lengths (Å) for CH_3ReO_3 Grafted onto Dehydrated Silica−Alumina, with DFT-Calculated Bond Distances for Two Models of CH_3ReO_3 Grafted onto an Aluminosilsesquioxane Cube

		EXAFS curve-fit[a]		DFT-calculated distances	
path	*N*	*R* (Å)	σ^2 (Å^2)	model **I**	model **II**
Re═O	2	1.69	0.0012	1.674	1.678, 1.681
Re═O	1	1.79	0.0016	1.788	1.789
Re−C	1	2.07	0.0012	2.082	2.096
Re−$O_{support}$	1	2.13	0.0056	2.260	2.172
Re−Al	1	3.06	0.0054	2.977	3.044

[a] The inner potential energies (ΔE_0) and global amplitude reduction factor (S_0^2) were fixed at 0.0 eV and 1.0, respectively, during the fit (see text). Coordination numbers were fixed at their integer values (*N*). Residual = 7.5.

an additional Re−Al path to account for the peak at 2.7 Å in *R*-space. To minimize the number of correlated parameters, coordination numbers were fixed at their integer values. Also, since the fitted values of S_0^2 and ΔE_0 for polycrystalline CH_3ReO_3 were insignificantly different from their starting points at 1.0 and 0.0 eV, respectively (see above), and since these parameters are not expected to be precisely the same for grafted CH_3ReO_3, their values were also held at their starting points. For each path, the distance (*R*) and Debye−Waller factor (σ^2) were refined sequentially.

The curve-fit improved significantly when the symmetry of the oxygen shell was relaxed. Two Re═O paths converged to the same distance, while the third was significantly elongated. However, the fit returned an unreasonably small Debye−Waller factor ($<1 \times 10^{-3}$ Å^2) for the longer Re═O path, Table S1. This result suggests the presence of an additional scatterer in the first coordination sphere. Inclusion of a fourth Re−O scattering path, presumed to involve an oxygen atom of the support, caused the Debye−Waller factors to assume physically meaningful values, comparable in magnitude to those obtained for polycrystalline CH_3ReO_3. The curve-fit and its associated fit parameters are shown in Figure 7 and Table 2, respectively. The fit and the experimental data match very well in both *k*-space and *R*-space. The model has only 10 adjustable parameters, well below the calculated N_{idp} value of 19 (from eq 2, with $2 \le k \le 14$ Å^{-1} and $0.6 \le R \le 3.2$ Å). The fit also matches the data well in the first coordination sphere when performed with k^1-weighting, Figure S2. However, this data treatment generates a less distinct second-coordination sphere peak, and it is therefore more difficult to judge the fit to the Re−Al path.

When coordination numbers for the EXAFS fit were allowed to vary (generating an additional five adjustable parameters, still within the limit of N_{idp} for this dataset), they produced integer values for all shells (±15%, well within the accepted error of the EXAFS technique), Table S3. Refinement of S_0^2 and ΔE_0 produced values of 0.98 and 0.48 eV, respectively (a total of 17 adjustable fit parameters); accompanying changes in the path lengths *R* and Debye−Waller factors σ^2 were insignificant (<0.01 Å and 0.0003 Å^2, respectively) relative to the curve-fit in which *N*, S_0^2, and ΔE_0 were not refined (Figure 7 and Table 2).

Finally, we investigated whether an additional oxygen shell or a multiple scattering interaction might be responsible for the EXAFS peak at ca. 2.7 Å. Both were ruled out by poor agreement between the curve-fits and the data. We also considered the possibility that this feature arises from a Re−Re path, caused by association of multiple CH_3ReO_3 groups on the silica−alumina surface. Direct interactions of CH_3ReO_3 are not observed in organic solvents, nor in polycrystalline CH_3ReO_3;[44] however, spontaneous polymerization of CH_3ReO_3 occurs in aqueous solution.[45] Curve-fitting to a model constructed from the structure of polymeric CH_3ReO_3 resulted in a physically implausible Re═O path length and an unreasonably large Debye−Waller factor for the Re−Re path, Table S4.

Computational Modeling. To probe the soundness of the EXAFS model reported in Table 2, we turned to computational analysis. First, the structure of the isolated CH_3ReO_3 molecule was minimized using DFT. Table 1 compares the calculated Re═O and Re−C distances with those obtained for polycrystalline CH_3ReO_3 by EXAFS (this work), as well as published results from gas-phase electron diffraction, and neutron powder diffraction on polycrystalline CH_3ReO_3. The high level of overall agreement establishes the legitimacy of our computational approach.

A DFT investigation of possible structures for grafted CH_3ReO_3 begins with the selection of a structural model for the silica−alumina support. Since silica−aluminas are amorphous with respect to their short- and long-range order, all models are necessarily approximate. Crystalline aluminosilicate frameworks, such as the zeolites, are not appropriate models, because their structures contain charge-compensating alkali cations and/or strongly acidic, bridging hydroxyl sites that are absent in amorphous silica−aluminas.[39] Periodic structures for crystalline silica have been used to represent amorphous silica in calculations.[46] However, we and others[47] have observed experimentally that CH_3ReO_3 does not adsorb strongly onto silica, nor does the resulting physisorbed material catalyze olefin metathesis. Crystalline aluminas are also inappropriate models because they lack the strong acidity of silica−alumina, which appears to be necessary for high catalytic activity in olefin metathesis. Indeed, many of the unique properties of silica−alumina as a catalyst support arise because it is neither an admixture of silica and alumina nor a poorly ordered aluminosilicate, but a solid solution that possesses both strong Lewis acidity (unlike silica) and strong Brønsted acidity (unlike alumina) without charge-compensating/exchangeable cations.

Structural information for amorphous silica−alumina is difficult to obtain, although neutron diffraction methods have recently provided insight on the distribution of Si−O−Si angles in amorphous silica.[48] Some parameters for silica−alumina have been obtained by ^{27}Al and ^{29}Si solid-state NMR[49−51] and Al XANES.[52] In fully dehydrated silica−aluminas with low alumina contents (≤32 wt % as Al_2O_3), the vast majority of Al sites are four-coordinate,[52,53] and they do not bear hydroxyl groups, either terminal or bridging.[54] Reversible changes to and from 6-fold coordination during chemisorption of water and

(45) Herrmann, W. A.; Fischer, R. W. *J. Am. Chem. Soc.* **1995**, *117*, 3223−3230.
(46) Ma, Q.; Klier, K.; Cheng, H.; Mitchell, J. W.; Hayes, K. S. *J. Phys. Chem. B* **2000**, *104*, 10618−10626.
(47) Zhu, Z.; Espenson, J. H. *J. Mol. Catal. A: Chem.* **1997**, *121*, 139−143.
(48) Tucker, M. G.; Keen, D. A.; Dove, M. T.; Trachenko, K. *J. Phys. Chem. Condens. Matter* **2005**, *17*, S67−S75.
(49) Oldfield, E.; Haase, J.; Schmitt, K. D.; Schramm, S. E. *Zeolites* **1994**, *14*, 101−109.
(50) McMillan, M.; Brinen, J. S.; Carruthers, J. D.; Haller, G. L. *Colloids Surf.* **1989**, *38*, 133−148.
(51) Doremieux-Morin, C.; Martin, C.; Brégault, J.-M.; Fraissard, J. *Appl. Catal.* **1991**, *77*, 149−161.
(52) Kato, Y.; Shimizu, K.; Matsushita, N.; Yoshida, T.; Satsuma, A.; Hattori, T. *Phys. Chem. Chem. Phys.* **2001**, *3*, 1925−1929.
(53) Omegna, A.; Van Bokhoven, J. A.; Prins, R. *J. Phys. Chem. B* **2005**, *109*, 9280−9283.
(54) Hunger, M.; Freude, D.; Pfeifer, H.; Bremer, H.; Jank, M.; Wendlandt, K.-P. *Chem. Phys. Lett.* **1983**, *100*, 29−33.

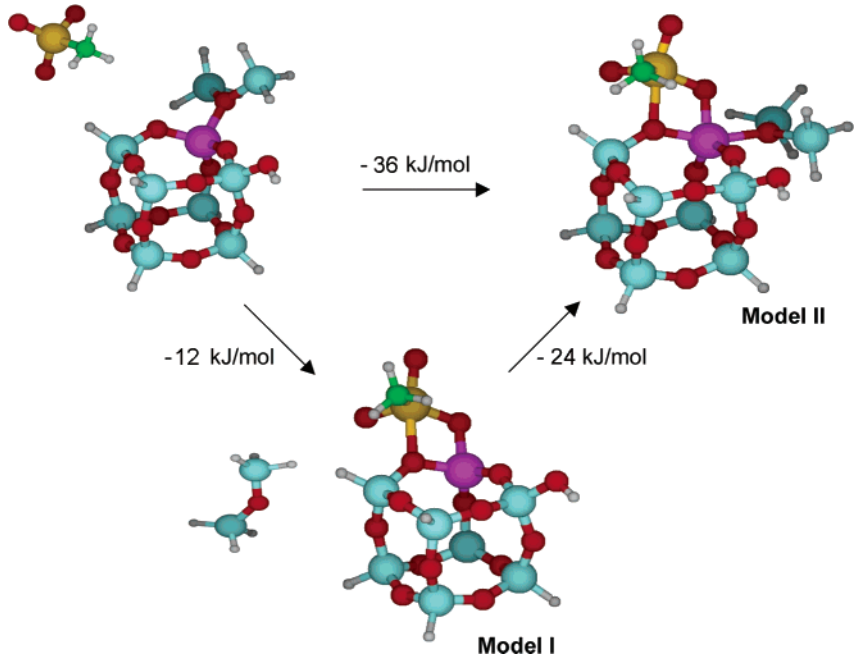

Figure 8. DFT-calculated reaction energies and structures for two models of the interaction between a siloxane-capped aluminosilsesquioxane monosilanol cube (representing the silica−alumina surface) and CH_3ReO_3. Separated molecules should be interpreted as infinitely separated. Color scheme: Re (yellow), Al (purple), Si (blue), O (red), C (green), H (white).

ammonia have been documented by ^{27}Al NMR[55] and Al K-edge XANES.[53] A minor component (<10 mol %) of tricoordinate Al has been identified in steamed zeolites,[56] which likely contain an amorphous silica−alumina component.[53] The Lewis acidity of amorphous silica−aluminas is believed to arise from the presence of coordinatively unsaturated Al sites,[57] while their Brønsted acidity is associated with terminal silanols located adjacent to these Al sites.[55]

A simple model cluster, $H_2Si(OH)OSi(OH)H_2$, has been used in computational modeling of a hypothetical CH_3ReO_3 grafting reaction by condensation, although the reaction was reported to be endothermic by 33 kJ/mol.[3] While such small clusters have often been used to model silica surface interactions with adsorbates,[58] they often allow more degrees of freedom in the structural minimization than are realistic for an oxide support via the torsional flexibility of the open chain, even when the end-points are held fixed during energy minimization. Furthermore, the high degree of H-capping in these models results in electronic properties that are quite different from those of silica, in which Si is coordinated exclusively by oxygen.

Cage-like structures, including the partially and fully condensed silsesquioxanes,[59] are better models for silica surfaces because of their constrained Si−O−Si angles[60,61] and because of their oxygen-rich nature. The analogy has been extended experimentally to aluminosilsesquioxane cubes, which were synthesized and characterized by single-crystal X-ray diffraction as models for silica−alumina and aluminum-modified silica surfaces.[62,63] Therefore an Al-substituted silsequioxane monosilanol was selected to model both Lewis and Brønsted acid sites on the surface of silica−alumina. The hydride-capped, all-Si version was modified by replacing one SiH corner with an Al atom, Figure 8. An additional siloxane ligand ($H_3SiOSiH_3$) was included in order to impose 4-fold coordination at Al (although this site is not tetrahedral, due to the constrained Si−O−Al angles of the cube, 115.6°). In the presence of a stronger Lewis base, the siloxane ligand could be displaced, modeling *latent* Lewis acidity in silica−alumina.[55]

After minimizing the energy of the aluminosilsesquioxane cube, CH_3ReO_3 was attached to determine its optimal binding geometry. Since a suitable empirical potential for Re was not available, starting geometries could not be determined by typical docking calculations. Instead, we compared the energies of plausible grafted forms of CH_3ReO_3. The structures we considered include coordination to the Re atom by the silanol oxygen or any of the bridging oxygens of the cube, hydrogen-bonding of the silanol to an oxo ligand of CH_3ReO_3, and coordination of an oxo ligand to the Al atom. Reaction of the methyl ligand with the silanol proton (i.e., to form a grafted perrhenate ester with liberation of methane) was not considered, since no methane was detected during CH_3ReO_3 grafting.

The most energetically favorable interaction of CH_3ReO_3 with the aluminosilsesquioxane cube model involves coordination at the Al corner. The cube prefers to bind CH_3ReO_3 rather than $H_3SiOSiH_3$ at this site, shown in Figure 8 as model **I**, by 12 kJ/mol. Calculated bond distances are summarized in Table 2. One of the oxygen atoms of CH_3ReO_3 interacts with the Al corner of the cube, at an O−Al distance of 1.873 Å. Substantial lengthening of this Re═O bond upon grafting, from 1.690 to 1.788 Å, suggests a reduction in its bond order. This Lewis acid−base interaction is reinforced by a second interaction

(55) Omegna, A.; Van Bokhoven, J. A.; Prins, R. *J. Phys. Chem. B* **2003**, *107*, 8854−8860.
(56) Van Bokhoven, J. A.; Van der Eerden, A. M. J.; Koningsberger, D. C. *J. Am. Chem. Soc.* **2003**, *125*, 7435−7442.
(57) Schwartz, J. A. *J. Vac. Sci. Technol.* **1975**, *12*, 321−323.
(58) Frash, M. V.; van Santen, R. A. *Top. Catal.* **1999**, *9*, 191−205.
(59) Feher, F. J.; Budzichowski, T. A. *Polyhedron* **1995**, *14*, 3239−3253.
(60) Civalleri, B.; Garrone, E.; Ugliengo, P. *Chem. Phys. Lett.* **1999**, *299*, 443−450.
(61) Sauer, J.; Hill, J.-R. *Chem. Phys. Lett.* **1994**, *218*, 333−337.
(62) Duchateau, R.; Harmsen, R. J.; Abbenhuis, H. C. L.; van Santen, R. A.; Meetsma, A.; Thiele, S. K.-H.; Kranenburg, M. *Chem. Eur. J.* **1999**, *5*, 3130−3135.
(63) Feher, F. J.; Budzichowski, T. A.; Weller, K. J. *J. Am. Chem. Soc.* **1989**, *111*, 7288−7289.

between Re and an adjacent, bridging oxygen of the cube (SiOAl). The interaction is slightly stronger with the more basic bridging oxygen on the OSi(H)OAl cube edge, at a Re−O bond distance of 2.260 Å and a Re−Si distance of 3.474 Å, compared to the OSi(OH)OAl edge. However, this is likely an artifact of H-termination in the model. There is ample experimental precedent for coordination of Lewis bases to the electrophilic Re(VII) center in CH_3ReO_3.[64−66] Association of CH_3ReO_3 with a Lewis acidic Al site is expected to make Lewis base coordination even more favorable. CH_3ReO_3 also formed a stable adduct with the cube by binding to the Al corner only (i.e., without interacting with an adjacent bridging O) or by hydrogen-bonding via an oxo ligand to the silanol corner, although each of these configurations was of considerably higher energy than model **I**.

Binding CH_3ReO_3 to the cube in the same geometry as in model **I** but without displacing the siloxane, i.e., by expanding the coordination number at Al to five (model **II**), is even more stable, with the total energy lowered by an additional 24 kJ/mol relative to model **I**. Similar changes in bond lengths upon grafting were predicted for model **II**. As expected, the O−Al distance involving the oxo ligand is longer (1.866 Å) in model **II** than in model **I**, as is the Re−Al distance, at 3.044 Å. However, the approach of Re to the bridging oxygen of the cube, at 2.172 Å, is closer in model **II**. These results are consistent with a less Lewis acidic Al site in model **II**, and consequently a more basic oxygen donor in the adjacent cube bridging site.

Changes in the atom charge densities, evaluated by the natural bond orbital (NBO) method as implemented in the Gaussian03 code, suggest that grafting results in charge transfer to the oxo ligand interacting with Al from the other two oxo ligands and the methyl carbon. This is consistent with a slight lengthening of the Re−C bond relative to the calculated structure for isolated CH_3ReO_3. There is a small change in the NBO-derived C and Re charges, from which we infer a charge transfer from C to Re (i.e., C becomes more positive, while Re becomes more negative). The NBO analysis also shows changes in the electronic structures of the Re and C atoms upon grafting. Re gains electron density in a (mostly) 5d orbital, whereas C loses electron density from a (mostly) 2p orbital.

Comparison of EXAFS and DFT-Calculated Structures. Fitted bond lengths from EXAFS are compared to the values calculated for both DFT models in Table 2. The agreement in the first three shells (i.e., the oxo and methyl ligands) is striking, particularly since the fit is highly constrained, with the coordination numbers, S_0^2 and ΔE_0 parameters all held fixed. In particular, the EXAFS-derived elongation of one Re═O path by 0.10 Å relative to the other two is reproduced in the Re═O distances predicted by DFT.

EXAFS curve-fitting was unable to distinguish between an Al or a Si scatterer in the second coordination sphere; both Re−Al and Re−Si paths resulted in reasonable fits. However, we suggest that Al is more likely to be responsible for the peak at 2.7 Å, because its flexible coordination number allows Al to interact directly with CH_3ReO_3. In contrast, a Si neighbor would not be expected to expand its coordination sphere to accommodate CH_3ReO_3, and indeed CH_3ReO_3 does not attach itself irreversibly to silica. Furthermore, the DFT models confirm that CH_3ReO_3 can engage in a highly favorable Lewis acid−base interaction with the Al site. The additional interaction of the organorhenium complex with an adjacent bridging oxygen of the SiOAl bond creates a two-point attachment of CH_3ReO_3 to the surface, anchoring Re at a fixed distance from Al and thereby decreasing the Debye−Waller factor for this path.

In the bond lengths of the shells representing interactions with the support (i.e., Re−$O_{support}$ and Re−Al paths), the EXAFS curve-fit shows reasonable agreement with both DFT models. Heterogeneity of the amorphous silica−alumina surface and the approximate nature of the cube model may contribute to the small differences. Nevertheless, we believe the agreement is better with model **II**, suggesting that most grafting events involve the formation of five-coordinate Al sites. This is consistent with the ^{27}Al MAS NMR results, which show that the ^{27}Al signal that disappears nearly completely upon dehydration of silica−alumina is not restored upon grafting CH_3ReO_3. Thus the low symmetry of the Al sites is preserved even after surface modification.

Conclusions

Spectroscopic and computational analyses concur that the Lewis acidic Al sites of silica−alumina represent the most favorable chemisorption sites for CH_3ReO_3 at low loadings. The interaction of the organometallic complex with the support results in elongation of one Re═O bond and coordination to Re of an adjacent bridging oxygen from the surface. The resulting two-point attachment creates a well-defined grafted site that is electronically distinct from its molecular precursor. The implications of these findings for the silica−alumina activation of CH_3ReO_3 toward olefin metathesis are under investigation.

Acknowledgment. We thank Dr. Dučanka Janečič and The Center for Molecular Modeling at the National Institute of Chemistry in Ljubljana, Slovenia, for use of their computing facility. We also thank Dr. R. L. Martin of Los Alamos National Laboratory for assistance with the DFT calculations, and particularly for providing valuable input on the theoretical treatment of Re. This work was funded by the U.S. Department of Energy, Basic Energy Sciences, Catalysis Science Grant No. DE-FG02-03ER15467. Portions of this research were carried out at the Stanford Synchrotron Radiation Laboratory, a national user facility operated by Stanford University on behalf of the U.S. Department of Energy, Office of Basic Energy Sciences. This work also made use of MRL Central Facilities supported by the MRSEC Program of the National Science Foundation under award No. DMR00-80034.

Supporting Information Available: Additional EXAFS curve-fits and Cartesian coordinates for DFT models. This material is available free of charge via the Internet at http://pubs.acs.org.

OM050962K

(64) Nabavizadeh, S. M. *Inorg. Chem.* **2003**, *42*, 4204−4208.
(65) Nabavizadeh, S. M.; Akbari, A.; Rashidi, M. *Eur. J. Inorg. Chem.* **2005**, *12*, 2368−2375.
(66) Wang, W.-D.; Espenson, J. H. *J. Am. Chem. Soc.* **1998**, *120*, 11335−11341.